Present-day stress field changes along the Baikal rift and tectonic implications

Carole Petit, Jacques Déverchère, and Frédérique Houdry

Géosciences Azur EP125, Université Pierre et Marie Curie, Villefranche-sur-Mer, France

Vladimir A. Sankov and Valentina I. Melnikova

Institute of the Earth's Crust, Russian Academy of Sciences, Irkutsk, Russia

Damien Delvaux

Royal Museum for Central Africa, Tervuren, Belgium

Abstract. Intraplate extension, in a frame of a global compressional stress field, seems linked to local lithospheric perturbations (lithospheric thinning or thickening) able to modify the resulting state of stress [Zoback, 1992]. The Baikal Rift Zone (BRZ), Siberia, is located north of the India-Asia collision zone and exhibits no direct communication with any oceanic domain. It can thus be fully considered as an area of continental extension, dominated by the "global compressional intraplate stress field" resulting from plate driving forces. In order to address the problem of its dynamics and kinematics and their links with the India-Asia collision, a comprehensive stress tensor analysis is presented, based on 319 focal mechanisms of earthquakes located along the whole Baikal rift. The stress field is varying at different scales of observation: when looking at central Asia (several thousands kilometers), the maximum horizontal stress S_{Hmax} directions remain rather constant (with a fan-shape geometry) when the tectonic regime goes from compressional (Himalayas) to extensional (Baikal). When observing the Baikal rift (about 1000 km long), clear variations of the stress regime are observed, from an extensional regime in the central part of the rift to wrench ones in its northern and southern ends. Finally, at the scale of 100 km, systematic S_{Hmax} reorientations occur close to major rift faults. We thus infer that the interaction between collisional processes and inherited structures may have a strong influence on rift dynamics. We then use computed stress tensors to predict slip vectors on major rift faults. Deformation patterns show two distinct parts of the rift: the South Baikal Rift (SBR) is characterized by a constant trending (around N100°E) slip vector, meanwhile the North Baikal Rift (NBR) exhibits a complex block rotation behavior involving at least three crustal blocks. We propose to interpret these surficial structures and motions as the result of an interaction between the regional compression coming from the India-Asia collision and the geometry of the hardly deformable Siberian platform. This particular setting can explain most of the surficial deformation patterns, which suggest a large-scale cracking of the lithosphere in the Baikal region. Other possible sources of stress could also be considered, like deep mantellic upwelling, or trench suction linked to the Pacific subduction.

Introduction

Relationships of the stress field to tectonics and structure of the upper lithosphere are complex and controlled both by local and regional factors. Stress field studies in active zones have widely developed within the last 10 years by means of in situ measurements, fault slip data and focal mechanisms. The World Stress Map Project [Zoback et al., 1989; Zoback, 1992] gathered informations on maximum horizontal stress orientations over the world, which were then compared to global models of plate motions. Although broad-scale (first-order) stress patterns appear to be the result of plate-driving forces [Bosworth et al., 1992; Richardson, 1992], it is shown that the addition of local second-order stresses, due for example to lithospheric flexure or buoyancy forces, may strongly affect the resulting stress field [Zoback, 1992].

More specifically, data collected inside continental areas show that in most cases, this first-order stress field is compressional. Continental extensional dynamics thus involves the influence of second-order stresses. For example, buoyancy stresses related to the existence of lithospheric heterogeneities (crustal and lithospheric thinning or thickening) may be of the same order of magnitude as first-order stresses induced by plate motions [Zoback et al., 1989; Zoback, 1992] and predominate upon them. This observation implies that continental extension occurs at the place where two independent phenomena of similar magnitude are superimposed, the first one resulting from plate-driving forces and the second one from local lithospheric perturbations. However, it is not clear whether these perturbations are a cause or an effect of rifting dynamics.

This matter of intracontinental rifting and its relationships to neighboring compressional areas is of special interest in the Baikal Rift Zone (BRZ) where active extensional tectonics extends over 1500 km, north of the India-Asia collision. The problem of the important positive relief associated with rifting has been partially addressed by gravity modelling, which shows the high effective elastic thickness of the lithosphere [Diament and Kogan, 1990; Ruppel et al., 1993; Burov et al., 1994]. Thus lithospheric flexure may be partly responsible for the elevated topography observed in the BRZ. Asthenospheric upwelling is also a possible agent of rifting process, although it seems small in the Northern Baikal Rift (NBR) [Burov et al., 1994; Petit and Déverchère, 1995]. Nevertheless, an asymmetric uplift of the asthenosphere seems located beneath the southern lake Baikal at

depths up to 50 km [Gao et al., 1994]. Concerning vertical movements of the lithosphere in the BRZ, the predominance of one of these factors upon the other is thus not clearly elucidated.

The large extent of the Baikal rift system, as well as the diversity of its structural orientations, allow us to study the interaction of the stress field with active faults and their links with the Asian velocity field. Analogical experiments [Tapponnier et al., 1982; Davy and Cobbold, 1988; Peltzer and Tapponnier, 1988] and horizontal kinematic models of central Asia [Avouac and Tapponnier, 1993] favor a direct link between the India-Asia collision and the existence of the BRZ. The particular S-shaped geometry of the rift, with en echelon disposition of faults and basins in the NBR, suggests that oblique extension resulting from extrusion processes may take a significant part in its opening. However, clear field evidence is scarce and concerns only Holocene cumulative displacements and recent Cenozoic microtectonic data [Houdry, 1994; D. Delvaux et al., Paleostress reconstructions and geodynamics of the Baikal region, Central Asia, II, Cenozoic tectonic stress and fault kinematics, submitted to Tectonophysics, 1996]. Instantaneous velocity field measurements by Global Positioning System (GPS) have been performed for the first time in the BRZ during the summer of 1994 [Petit et al., 1994] and will provide the first results in 1997. From the already available information, several questions are worth pointing out: what are the characteristics of the stress field in the Baikal region and which links can be drawn between it and the India-Asia collision? Is the direction of the maximum horizontal stress consistent with the velocity field within deforming Asia? How does the present-day rift deformation relate to the Asian strain field? Detailed imaging of the present-day stress field in the rift zone should allow us to shed light on these points and better constrain the dynamics and kinematics of the rift. The numerous data used here (319 focal mechanisms, see Plate 1) make the Baikal rift the best-documented active rift system in the world. In the present paper, we use this comprehensive data set of fault plane solutions in order to determine the stress field characteristics in different parts of the rift and try to correlate them with regional stress patterns of Asia. Using these results, and assuming that the slip vector on a given fault results from the combined effect of the local stress field and the fault geometry, we predict the displacement field on the basis of accurate field and satellite data on major rift faults, and infer a qualitative model of deformation of the rift area.

From Individual Strain Observations to Regional Stress Field

Inversion Methods and Selection of Nodal Planes

Several indicators may be used to determine the stress field, such as in situ measurements, which allow us to constrain the local tectonic stress in both orientation and magnitude [see e.g., Shamir et al., 1988; Cornet and Burlet, 1992; Rebaï et al., 1992], observation of tectonic structures like striated fault planes [see e.g., Angelier, 1979; Rebaï et al., 1992; Hippolyte et al., 1994], and focal mechanisms of earthquakes [see e.g., McKenzie, 1969; Michael, 1987; Hartse et al., 1994]. The use of fault plane solutions for stress inversion implies homogeneous data sets and the choice of the actual fault plane among the two proposed nodal planes [Michael, 1987; Horiuchi et al., 1995]. Its advantage is the abundance of data in seismic zones where other informations

(i.e., microtectonic measurements) are scarce. Focal mechanisms give the slip vector on two possible fault planes, only one of which is the actual seismic fault. If the stress tensor is given and triaxial, only the actual fault plane will give a slip vector consistent with the stress tensor. If not, superimposition of compressional and tensional quadrants of several focal mechanisms in a given area will provide compressional and tensional zones where the maximal and minimal stress axes have to be searched [Angelier and Mechler, 1977]. This first estimation of the stress tensor is often enough to discriminate between the two nodal planes of each mechanism, and allows creation of a preferred set of planes representing seismic faults. Inversion methods are then used to minimize the deviation between observed and calculated striations, in order to refine the stress tensor determination [see e.g., Gephart and Forsyth, 1984; Carey-Gailhardis and Mercier, 1987; Rivera and Cisternas, 1990]. Nevertheless, the choice of the likely failure plane remains sometimes ambiguous and does not avoid, when possible, a comparison with strike and dip of active faults on the field.

In order to refine this discrimination, we compare in this study the results obtained by the use of two numerical methods [Carey-Gailhardis and Mercier, 1987; Delvaux et al., 1996]. Both algorithms involve three similar steps. The first step is the estimation of main stress axes directions by the right dihedra method of Angelier and Mechler [1977]. Then, applying this initial tensor to the whole data set, the selection of preferred fault planes is made using different criteria (see after). Finally, an inversion procedure (in a least squares sense) provides the new tensor, using the preferred set of data, by the adjustment of several possible parameters, among which are the slip deviation, that is the difference between calculated and observed slip vector orientation, used in both methods, and the friction coefficient, used in the Delvaux et al. [1996] routine.

To select the best-fitting fault plane, Carey-Gailhardis and Mercier [1987] use the following criteria: the deviation between calculated and observed slip vectors which must be less than 20°, and the R ratio for each fault plane, where $R=(\sigma_2-\sigma_1)/(\sigma_3-\sigma_1)$, must range between 0 and 1. When the stress tensor is well defined, these criteria are theoritically accurate enough to distinguish the fault plane from the auxiliary one. In the present case, additional information such as geological microtectonic data would help greatly to constrain this discrimination, but the uncertainties on hypocenter locations, as well as the high fracture density, do not allow association of nodal planes with well-known fault tracks. Thus, in order to control this determination, we also use the program of Delvaux et al. [1996] which computes the internal friction coefficient μ for each fault plane and compares it with fracture criteria values described by the expression of the Mohr envelopes:

$$\sigma_s = COH + \mu\sigma_n \tag{1}$$

Where σ_s and σ_n are the shear and normal stresses, respectively. COH describes the cohesion of the rock, and μ is the coefficient of internal friction, which is equal to $\tan(\Omega)$ where Ω is the angle of internal friction.

This describes the ability of the tensor to activate or not activate preexisting fractures: the fault plane is activated only if its position on the Mohr diagram is above the envelope. This criterion may be of delicate use because of the lack of knowledge on the mechanical and rheological state of the rocks. Zoback and

Beroza [1991] have shown that near-lithostatic pore pressure may significantly reduce the resistance to fault motion. However, as reported later, comparing the preferred sets of planes selected with this parameter or with the slip deviation criteria allows us to give an estimate of the accuracy of stress tensor determination.

Data Set: Selection and Uncertainties of Stress Inversion

We use a total database of 319 focal mechanisms provided by different sources and recorded between 1950 and 1994 (Table 1). Magnitudes range between 2.8 and 7.8. Russian solutions represent the major part of the data set, involving 308 mechanisms, among which 161 are composite solutions. Thirteen other mechanisms come from waveform modelling made by *Doser* [1991a,b]. Finally, 11 mechanisms are Centroid Moment Tensor Solutions (CMTS) determined with the method of *Dziewonski and Woodhouse* [1983]. The geographical distribution of fault plane solutions is shown on Plate 1. Fourteen focal mechanisms of the Russian data set were also determined by other procedures: waveform modelling [*Doser*, 1991a,b] or CMT determinations (Table 1). In most cases, the discrepancies between these determinations are small: angular differences on P and T axis are less than 20° for 85% of the solutions. We have generally considered that waveform modelling (especially CMT) solutions are more accurate, except for the Mondy earthquake of April 4, 1950, for which the only consistent solution is given by the first motion determination [*Solonenko*, 1977].

Single focal mechanisms represent 151 nonambiguous solutions of a comprehensive Russian database of 40 years of seismicity [*Solonenko et al.*, 1993]. We applied here the procedure used by *Déverchère et al.* [1993] to select these reliable mechanisms. Composite solutions are numerous in our data set (50%) and often subject of suspicion in seismological studies, mainly because they rely on the additional assumption that several nearby earthquakes depict the same fault motion. An ideal way to avoid this problem is to compute the stress tensor using only first motion readings, without previous fault plane determinations [*Rivera and Cisternas*, 1990]. Nevertheless, it has been demonstrated that earthquakes occurring in a wide area, on randomly oriented faults, may statistically help to constrain the principal stress axes [*Xu et al.*, 1992]. In other words, when constructing composite fault plane solutions with a large number of data, the variations of P and T axes due to local fault geometries cancel each other. The resulting "best-fitting" P and T axes hence represent a good estimation of the maximal and minimal stresses, respectively. Stress tensor determinations by the superimposition of tensional and compressional dihedrons act in the same way. We thus believe that well-constrained composite solutions are reliable, and represent an important amount of information on the local stress field. Each composite solution selected in this study is made of nearby earthquakes grouped inside a 10x10 km area, with compatible first P-wave arrivals (including an important amount of direct waves) at the same stations. Uncertainties on focal depths are ranging within 5-10 km and do not significantly affect first motion distribution on the focal spheres. These conditions allow us to consider a group of similar shocks as if it was an individual event.

The data set has been geographically divided into 15 subareas (Figure 1) used for stress tensor determination. It is supposed that the size and position of the different subregions can influence each corresponding stress tensor. Indeed, it appears that resizing the subregions may slightly modify the computed stress tensor.

Actually, two simple alternatives arise: either the stress field changes continuously, and the result will be a representative average of the stress field in the selected area, if the latter is small enough compared to the scale of stress patterns; or stress field variations are strong and discrete, and the result will be associated with a variable amount of incompatible focal mechanisms if the chosen subregion is poorly positioned. An a posteriori control on rejected solutions is thus needed in order to insure the validity of the subsets. We made the choice to separate the data set taking into account the main active features for a given area: each subregion tends to include the entire length of main active faults (Figure 1) because stress tensors applied to each structural feature are supposed to be homogeneous. A last limitation when choosing the size of subregions is the data density. A percentage of selected solutions is presented in Table 2, showing that about 85% of the focal mechanisms are compatible with the obtained tensors.

Finally, we performed a test on the validity of the data set (especially on composite solutions) in the Muyakan area (Figure 1). This region has been the subject of stress tensor determination by *Déverchère et al.* [1993]: first motions of 39 small magnitude (2.2-4.4) earthquakes recorded between 1977 and 1980 were used to determine accurate single fault plane solutions and a stable extensional stress tensor. In the present study, we use in the same area 43 focal mechanisms, among which 35 are composite solutions and 8 are single focal solutions coming from moderate magnitude (2.8-5.7) events. This region thus provides the opportunity to test the consistency of our data and to estimate the reliability of composite solutions. Table 3 compares our stress tensor determination to that of *Déverchère et al.* [1993]. Despite of the use of different samples, the computed stress tensors remain quite similar: horizontal stress directions are identical to within 4°, and resulting R values are equal (Table 3 and Figure 2). Magnitude differences between both earthquake samples thus do not appear to affect the result of stress tensor inversion. Moreover, composite solutions seem to statistically constrain the stress field with rather good accuracy.

How far do uncertainties on data set (choice of fault planes) and on computing (minimization procedures) affect the final inversion? The *Carey-Gailhardis and Mercier* [1987] and the *Delvaux et al.* [1996] methods are compared in order to depict the stability of the obtained stress tensors (Figure 2). In most cases, these methods lead to the selection of similar sets of nodal planes (divergent choices are made for about 8% of the planes). They also lead to similar stress directions, especially for σ_2 and σ_3 whose orientations are better constrained because they are often nearly horizontal. Differences between these two determinations are thought to be a good estimate of uncertainties on stress computations, but do not represent actual errors, which also depend on the data density. Consequently, an average tensor solution is deduced from both solutions computed for each subset (Table 2). Differences between this average and one or the other solution are supposed to reflect computational uncertainties on dip and plunge of each axis and on R value. A quality factor is assigned to each result, depending on the total number of data and on the number of solutions kept for the inversion (Table 2), in order to evaluate their relative reliability.

Results of Stress Tensor Determination

A stress tensor can be described either in terms of stress orientation, or in terms of tectonic regime. The latter is presented

Table 1. List of the 319 Fault Plane Solutions Used in This Study, Grouped into 15 Subsets

Date / Information	Latitude	Longitude	Strike	Dip	Rake	Magnitude	Origin
			Region: Bolnai				
630601	49.60	99.50	100	26	90	4.5	Irkutsk
670607	49.50	97.20	60	58	130	5.0	Novosibirsk
750821	49.63	97.38	240	71	-29	4.5	Irkutsk
750925	49.57	98.35	74	45	104	4.5	Novosibirsk
770929	49.66	97.88	351	45	96	4.5	Novosibirsk
781112	49.08	99.72	92	45	139	4.4	Novosibirsk
791213	49.62	97.88	326	45	-34	4.5	Novosibirsk
830409	49.21	97.94	201	50	-124	3.5	Irkutsk
860407	49.47	98.90	28	50	-98	4.5	Irkutsk
861212	49.62	99.86	24	70	82	2.8	Irkutsk
890203	49.61	97.41	111	41	108	4.5	Novosibirsk
890515	49.72	97.86	225	45	94	4.5	Novosibirsk
Composite	49.68	97.26	209	78	-37		Irkutsk
Composite	49.54	97.15	62	86	-97		Irkutsk
Composite	49.55	97.56	14	82	-153		Irkutsk
Composite	49.45	97.19	271	54	87		Irkutsk
Composite	49.33	98.45	196	30	14		Irkutsk
Composite	49.46	98.46	14	53	74		Irkutsk
Composite	49.39	98.01	283	50	63		Irkutsk
			Region: Busingol				
660510	51.70	98.92	265	70	15	5.8	Irkutsk
720527	51.37	98.05	61	45	146	4.5	Novosibirsk
741129	51.79	98.47	137	45	157	5.2	Novosibirsk
760401	51.06	98.03	148	80	166	5.5	Irkutsk
780831	50.93	98.53	47	58	-22	4.5	Irkutsk
831120	51.31	98.38	78	67	-53	4.5	Novosibirsk
Composite	51.05	98.01	22	44	-153	4.0	Irkutsk
Composite	51.00	98.00	315	84	127		Irkutsk
Composite	51.06	98.19	69	56	69		Irkutsk
Composite	51.01	97.98	230	64	136		Irkutsk
Composite	51.00	98.22	254	62	42		Irkutsk
Composite	51.14	98.18	47	58	-22		Irkutsk
Composite	51.12	97.96	236	82	21		Irkutsk
Composite	50.95	98.05	198	72	21		Irkutsk
Composite	51.83	98.35	86	87	-10		Irkutsk
Composite	50.36	98.05	264	50	76		Irkutsk
Composite	51.75	98.33	107	70	48		Irkutsk
			Region: Khubsugul				
760401	50.62	100.22	293	48	72	4.5	Irkutsk
850406	51.36	100.61	25	48	-102	4.8	Irkutsk
850824	51.20	100.40	0	44	-126	4.0	Irkutsk
870308	51.30	100.36	348	56	-117	4.0	Irkutsk
Composite	51.44	99.82	70	85	-50		Irkutsk
Composite	51.74	100.35	240	20	28		Irkutsk
Composite	51.36	100.62	235	47	-90		Irkutsk
Composite	51.69	100.83	325	52	94		Irkutsk
			Region: Transbaikal				
570206*	50.12	105.32	154	80	-10	6.5	Doser
580623	48.70	103.20	1	70	151	6.2	Irkutsk
611009	51.50	104.80	10	56	-150	3.5	Irkutsk
630423	47.00	103.60	217	34	178	5.0	Irkutsk
670105	48.10	102.90	13	88	171	7.8	Irkutsk
670105	47.95	103.00	351	69	174	5.0	Irkutsk
670107	48.00	103.00	13	41	-150	5.0	Irkutsk
670118	47.90	102.90	30	70	111	5.0	Irkutsk
670120	48.10	103.10	348	62	170	7.0	Irkutsk
670603	49.20	104.00	36	56	150	4.5	Irkutsk
741218	48.35	103.15	255	86	-38	5.4	Irkutsk
840805	49.10	101.29	174	80	126	4.8	Irkutsk
870301	49.78	102.45	52	40	-100	5.2	Irkutsk
890513	50.18	105.39	206	84	162	5.0	Irkutsk

Table 1. (continued)

Date / Information	Latitude	Longitude	Strike	Dip	Rake	Magnitude	Origin
Region: Sayan							
500404*	51.80	101.00	282	24	90	7.0	Irkutsk
620122	52.40	100.40	187	32	99	5.5	Irkutsk
800723	52.32	102.63	80	62	-123	4.5	Irkutsk
811201	52.18	101.00	203	40	-168	5.0	Irkutsk
Composite	51.74	100.35	240	20	28		Irkutsk
Composite	51.69	100.83	325	52	94		Irkutsk
Composite	51.86	101.16	314	44	93		Irkutsk
Composite	51.84	101.04	269	36	-95		Irkutsk
Composite	51.74	101.41	307	35	88		Irkutsk
Composite	51.78	101.40	315	52	-40		Irkutsk
Composite	51.74	101.44	336	50	-92		Irkutsk
Composite	51.71	101.38	32	40	-121		Irkutsk
Composite	51.62	101.32	218	71	-40		Irkutsk
Composite	51.66	101.75	225	34	31		Irkutsk
Composite	51.68	101.94	15	46	-149		Irkutsk
Composite	51.78	101.92	289	54	75		Irkutsk
Composite	51.69	102.04	84	70	-36		Irkutsk
Composite	51.71	102.21	16	35	-114		Irkutsk
Composite	51.86	102.81	4	88	-146		Irkutsk
Region: Southern Baikal							
590829*	52.64	106.90	248	53	-50	6.8	Doser
600312	52.00	105.80	210	50	-93	4.5	Irkutsk
600519	52.10	105.70	210	50	-93	4.0	Irkutsk
610807	52.40	106.60	15	50	-133	4.0	Irkutsk
611009	51.50	104.80	10	56	-150	3.5	Irkutsk
630210	52.60	106.80	33	50	-114	5.0	Irkutsk
660830	51.69	104.49	255	62	26	5.5	Irkutsk
670119	52.10	106.40	42	37	-99	4.0	Irkutsk
670211	52.09	106.46	218	67	168	5.3	Doser
700328	52.20	105.92	82	54	4	5.5	Irkutsk
700813	51.95	105.53	37	40	-113	4.9	Irkutsk
800206	51.74	105.14	217	80	-95	4.9	Irkutsk
800730	52.61	106.92	17	68	-101	4.5	Irkutsk
800926	51.86	105.33	68	18	-106	4.5	Irkutsk
810522*	52.05	106.32	18	18	-137	5.4	CMTS
820727	52.43	106.65	211	56	-68	4.7	Irkutsk
831124	52.99	106.95	220	80	-114	4.5	Irkutsk
850310	52.70	106.98	25	64	-105	4.8	Irkutsk
850325	52.27	106.43	317	40	-137	4.5	Irkutsk
850903*	52.85	106.87	343	82	-167	4.4	Doser
870329	52.19	106.20	58	40	-55	4.0	Irkutsk
870511	51.71	105.28	40	66	-86	4.8	Irkutsk
890513*	52.20	105.93	206	70	-174	5.8	CMTS
Composite	51.59	104.53	255	62	-24		Irkutsk
Composite	51.79	105.23	40	30	-110		Irkutsk
Composite	51.87	105.18	94	28	-54		Irkutsk
Composite	52.00	105.59	37	40	-112		Irkutsk
Composite	52.17	105.80	350	86	145		Irkutsk
Composite	52.17	105.83	171	54	-121		Irkutsk
Composite	52.21	106.38	80	51	-100		Irkutsk
Composite	52.02	106.32	66	52	-48		Irkutsk
Composite	52.40	106.75	21	42	-112		Irkutsk
Composite	52.56	106.97	44	49	-96		Irkutsk
Composite	52.53	106.91	0	66	-156		Irkutsk
Region: Central Baikal							
611028	53.60	108.80	4	42	-124	5.5	Irkutsk
620813	53.70	108.50	32	40	-117	5.2	Irkutsk
621028	53.60	108.60	8	44	-120	3.5	Irkutsk
630131	53.10	107.70	22	67	-117	4.0	Irkutsk
660403	54.00	108.60	37	33	-122	4.5	Irkutsk
720809	52.80	107.73	225	60	-102	5.2	Irkutsk

Table 1. (continued)

Date / Information	Latitude	Longitude	Strike	Dip	Rake	Magnitude	Origin
820128	53.49	108.69	52	54	-81	4.6	Irkutsk
841209	53.83	108.59	17	30	-117	4.8	Irkutsk
871224	52.97	107.37	19	34	-100	4.4	Irkutsk
871224	52.96	107.40	335	42	-126	4.5	Irkutsk
900520	53.07	108.02	197	42	-131	4.6	Irkutsk
920214	53.88	108.87	248	33	-66	5.4	Irkutsk
Composite	52.85	107.04	321	32	-65		Irkutsk
Composite	53.23	107.75	80	33	-65		Irkutsk
Composite	53.15	107.72	22	67	-117		Irkutsk
Composite	53.37	108.33	17	60	-88		Irkutsk
Composite	53.38	108.34	53	56	-105		Irkutsk
Composite	53.42	108.24	56	38	-74		Irkutsk
Composite	53.62	108.19	3	46	-98		Irkutsk
Composite	53.76	108.92	28	41	-112		Irkutsk
Composite	52.85	107.04	321	32	-65		Irkutsk
Region: Barguzin							
610727	54.10	110.00	221	62	-64	4.8	Irkutsk
620111	54.50	111.00	204	40	-101	2.8	Irkutsk
630205	54.30	111.40	37	50	-104	4.0	Irkutsk
630214	54.80	111.90	228	50	-105	3.3	Irkutsk
630215	55.20	111.00	30	65	-106	4.5	Irkutsk
630411	54.40	111.40	38	50	-112	3.5	Irkutsk
770824	54.12	110.44	192	46	-121	5.0	Irkutsk
790110	55.43	111.44	190	51	-116	5.0	Irkutsk
790110	55.40	111.43	257	62	-90	5.0	Irkutsk
790211	55.42	111.44	205	60	-109	3.5	Irkutsk
791205	55.32	111.39	219	51	-102	4.5	Irkutsk
800404	54.67	109.80	21	30	-90	4.5	Irkutsk
810527*	54.03	109.42	251	67	-87	5.2	CMTS
820114*	54.76	110.28	206	80	174	4.9	Doser
850223	55.37	111.33	22	52	-74	4.0	Irkutsk
850815	54.65	110.16	6	42	-97	4.0	Irkutsk
860122	55.46	109.37	10	50	-114	4.6	Irkutsk
870221	54.40	110.33	176	33	-114	4.9	CMTS
871008	55.29	109.60	112	40	-42	4.0	Irkutsk
890703	53.91	110.32	229	42	-108	4.5	Irkutsk
910912	54.68	110.70	28	67	-101	5.2	CMTS
Composite	53.88	109.02	172	42	-113		Irkutsk
Composite	54.98	109.46	2	70	-104		Irkutsk
Composite	55.33	109.62	28	46	-76		Irkutsk
Composite	54.71	110.98	35	36	-100		Irkutsk
Composite	54.73	111.04	12	58	-117		Irkutsk
Composite	54.26	110.67	33	34	-114		Irkutsk
Composite	53.77	110.21	29	42	-129		Irkutsk
Composite	55.00	111.54	28	30	-115		Irkutsk
Composite	54.79	111.93	36	32	-101		Irkutsk
Composite	54.32	111.30	23	43	-117		Irkutsk
Composite	54.32	111.30	39	49	-113		Irkutsk
Composite	54.32	111.30	40	50	-101		Irkutsk
Composite	54.31	111.39	51	85	-98		Irkutsk
Composite	54.31	111.45	51	48	-24		Irkutsk
Composite	55.17	111.04	33	50	-110		Irkutsk
Composite	55.24	110.92	1	55	-108		Irkutsk
Composite	55.18	110.19	310	55	-100		Irkutsk
Composite	55.26	110.06	194	20	-95		Irkutsk
Composite	55.15	110.19	19	86	-44		Irkutsk
Composite	55.02	110.70	29	38	-102		Irkutsk
Composite	55.25	111.17	16	49	-112		Irkutsk
Composite	55.38	111.45	190	51	-117		Irkutsk
Region: Kitchera							
611123	55.85	110.15	78	50	-90	4.5	Irkutsk
661231	55.60	110.80	205	39	-97	4.0	Irkutsk

Table 1. (continued)

Date / Information	Latitude	Longitude	Strike	Dip	Rake	Magnitude	Origin
670115	55.60	110.80	200	46	-130	5.2	Irkutsk
680617	55.96	110.58	69	56	-136	4.5	Irkutsk
720104	55.82	110.56	80	52	-100	4.5	Irkutsk
760923	55.75	110.54	37	68	-140	5.0	Irkutsk
821003	55.98	110.91	219	64	-124	4.5	Irkutsk
901026*	56.26	110.62	214	56	-150	5.1	CMTS
Composite	55.82	110.12	222	36	-125		Irkutsk
Composite	55.81	110.24	71	54	-97		Irkutsk
Composite	55.90	110.96	75	78	-93		Irkutsk
Composite	55.82	110.66	76	58	-101		Irkutsk
Composite	55.72	110.59	37	68	-141		Irkutsk
Composite	55.73	110.57	17	54	-123		Irkutsk
Composite	55.61	110.71	215	60	-104		Irkutsk
			Region: Tsipa				
680721	55.18	113.45	71	70	-95	5.0	Irkutsk
730616	54.85	112.58	194	44	-122	5.1	Irkutsk
860520	55.25	113.35	278	64	-123	4.0	Irkutsk
900718	54.96	112.23	206	47	-111	4.5	Irkutsk
Composite	54.87	112.50	43	50	-87		Irkutsk
Composite	55.24	113.21	53	30	-109		Irkutsk
Composite	55.25	113.33	74	73	-94		Irkutsk
Composite	55.38	113.58	26	52	-102		Irkutsk
			Region: Upper Angara				
630115	55.80	112.90	210	65	-127	3.5	Irkutsk
630312	56.10	111.50	57	61	-104	3.5	Irkutsk
630318	56.00	112.20	92	36	-90	3.5	Irkutsk
631201	55.90	112.00	28	26	-106	4.9	Irkutsk
671016	55.90	111.10	68	58	-112	4.0	Irkutsk
681126	55.90	111.49	264	55	-91	5.3	Irkutsk
761102	56.19	111.59	32	50	-123	5.2	Irkutsk
770604	56.20	111.82	22	22	-132	4.7	Irkutsk
790221	55.84	111.31	92	53	-98	4.0	Irkutsk
790701	55.66	112.30	259	74	-128	4.0	Irkutsk
810225	56.22	111.57	46	54	-56	4.5	Irkutsk
810303	55.73	112.88	65	50	-98	4.2	Irkutsk
810531	56.17	111.76	189	50	-120	4.5	Irkutsk
851111	55.63	112.01	327	54	-118	4.2	Irkutsk
881216	56.08	111.66	68	54	-20	4.0	Irkutsk
Composite	55.98	111.53	264	55	-91		Irkutsk
Composite	55.96	111.25	73	58	-99		Irkutsk
Composite	55.51	111.43	31	43	-109		Irkutsk
Composite	55.60	111.96	205	46	-94		Irkutsk
Composite	56.15	112.30	56	50	-111		Irkutsk
Composite	56.36	112.55	33	41	-125		Irkutsk
Composite	56.23	112.44	198	21	-116		Irkutsk
Composite	56.24	112.69	26	44	-133		Irkutsk
Composite	55.81	113.00	50	48	-111		Irkutsk
			Region: Muyakan				
620810	56.50	113.80	221	50	-101	3.3	Irkutsk
621111	55.84	113.22	215	58	-78	5.7	Doser
681108	56.14	113.75	204	47	-107	4.5	Irkutsk
740701	56.09	113.81	262	80	88	5.0	Irkutsk
781021	56.31	113.24	17	67	66	2.8	Irkutsk
790415	56.33	113.42	269	70	-121	4.0	Irkutsk
840202	55.93	113.68	96	44	-100	4.0	Irkutsk
880604	55.87	113.18	54	35	35	4.3	Irkutsk
Composite	56.38	113.33	270	15	-94		Irkutsk
Composite	56.34	113.31	61	46	-111		Irkutsk
Composite	56.33	113.34	299	39	-134		Irkutsk
Composite	56.31	113.51	267	88	-19		Irkutsk
Composite	56.16	113.45	86	62	-92		Irkutsk
Composite	56.32	113.60	80	76	-93		Irkutsk

Table 1. (continued)

Date / Information	Latitude	Longitude	Strike	Dip	Rake	Magnitude	Origin
Composite	56.30	113.15	234	78	-104		Irkutsk
Composite	56.14	113.19	35	66	73		Irkutsk
Composite	56.33	113.51	253	44	-115		Irkutsk
Composite	56.27	113.49	4	80	-74		Irkutsk
Composite	56.31	113.51	255	52	-110		Irkutsk
Composite	56.29	113.42	280	66	-116		Irkutsk
Composite	56.34	113.46	258	39	-155		Irkutsk
Composite	56.31	113.53	342	8	81		Irkutsk
Composite	56.20	113.61	220	83	-30		Irkutsk
Composite	56.20	113.39	254	84	-94		Irkutsk
Composite	56.21	113.51	225	50	180		Irkutsk
Composite	56.39	113.83	70	58	-103		Irkutsk
Composite	56.39	113.81	225	30	-22		Irkutsk
Composite	56.33	113.87	247	36	-96		Irkutsk
Composite	56.20	113.91	70	66	-100		Irkutsk
Composite	56.19	113.84	69	76	-90		Irkutsk
Composite	56.21	113.93	15	27	-146		Irkutsk
Composite	56.09	113.91	220	17	-106		Irkutsk
Composite	56.04	113.70	78	29	-113		Irkutsk
Composite	56.05	113.73	69	62	-117		Irkutsk
Composite	56.04	113.73	267	13	-160		Irkutsk
Composite	56.02	113.73	229	33	-113		Irkutsk
Composite	55.86	113.26	87	85	-96		Irkutsk
Composite	55.98	113.69	48	50	-96		Irkutsk
Composite	55.79	113.46	54	53	-90		Irkutsk
Composite	55.95	113.93	65	66	-118		Irkutsk
Composite	56.00	113.41	79	31	-104		Irkutsk
Composite	55.81	113.00	50	48	-111		Irkutsk
Composite	55.82	114.00	56	63	-101		Irkutsk
			Region: Muya				
570627*	56.20	116.54	120	80	-40	7.8	Doser
680831	56.40	115.78	245	60	-107	5.0	Irkutsk
711218	56.19	114.21	78	84	-97	5.0	Irkutsk
771120	56.55	115.78	71	55	-99	4.0	Irkutsk
860517	56.06	114.84	351	64	-142	3.5	Irkutsk
860526	56.26	116.19	120	46	83	4.2	Irkutsk
880621	56.07	114.68	347	29	-127	4.0	Irkutsk
Composite	56.09	114.02	34	65	-96		Irkutsk
Composite	56.23	114.14	78	84	-97		Irkutsk
Composite	56.41	114.28	268	15	-112		Irkutsk
Composite	56.34	114.42	49	72	-106		Irkutsk
Composite	56.12	114.51	30	41	-108		Irkutsk
Composite	56.18	114.85	31	51	-113		Irkutsk
Composite	56.18	114.87	68	72	-95		Irkutsk
Composite	56.32	115.51	45	26	-112		Irkutsk
Composite	56.29	115.50	248	28	-99		Irkutsk
Composite	56.25	116.51	68	55	-91		Irkutsk
Composite	56.20	116.76	322	56	-109		Irkutsk
Composite	56.28	116.39	6	44	135		Irkutsk
Composite	56.21	116.37	59	39	-91		Irkutsk
			Region: Tchara				
620423	56.50	117.20	210	52	-119	3.3	Irkutsk
700515	56.84	117.74	193	72	176	5.5	Irkutsk
700518	56.87	117.87	76	10	-90	4.8	Irkutsk
740621	56.35	117.70	40	58	-133	5.1	Irkutsk
750206	56.41	117.89	236	79	-51	4.7	Irkutsk
810117	56.36	117.94	21	45	-141	5.1	Irkutsk
840619	56.45	118.25	66	56	-64	4.7	Irkutsk
891205	56.67	117.99	186	42	-69	4.5	Irkutsk
940821	56.57	117.85	43	47	-104	6.0	CMTS
Composite	56.48	117.17	86	64	2		Irkutsk
Composite	56.48	117.19	129	62	-100		Irkutsk

Table 1. (continued)

Date / Information	Latitude	Longitude	Strike	Dip	Rake	Magnitude	Origin
Composite	56.69	117.33	229	43	-107		Irkutsk
Composite	56.67	117.37	32	34	-148		Irkutsk
Composite	56.60	117.74	50	35	-101		Irkutsk
Composite	56.60	117.78	311	44	74		Irkutsk
Composite	56.62	117.73	256	54	-107		Irkutsk
Composite	56.37	117.47	70	69	-116		Irkutsk
Composite	56.27	117.72	31	64	-109		Irkutsk
Composite	56.41	117.58	40	58	-131		Irkutsk
Composite	56.39	118.12	28	62	-113		Irkutsk
Composite	56.40	118.18	24	48	-60		Irkutsk
Composite	56.68	118.28	68	80	-35		Irkutsk
Composite	56.18	117.30	83	47	-117		Irkutsk
			Region: Eastern rift				
580105*	56.51	121.11	257	50	-100	6.5	Doser
580914*	56.61	121.06	63	63	-75	6.3	Doser
670118*	56.54	120.93	59	66	-166	6.0	Doser
710617	56.10	123.60	264	73	-8	5.7	Doser
720115	57.50	121.10	102	62	-61	4.8	Irkutsk
721125	56.19	123.56	45	74	-169	5.0	Doser
870707*	56.67	121.59	260	27	-90	5.3	CMTS
890420	57.03	121.23	101	82	33	6.3	CMTS
890429	57.13	121.80	91	87	-17	5.4	CMTS
890507	57.04	122.28	3	76	18	4.5	Doser
890517	57.07	122.03	277	77	-43	6.0	CMTS

See Figure 2 for geographical positions of the subregions. "Irkutsk" and "Novosibirsk" origins correspond to Russian publications of focal mechanisms from both Institutes [see e.g., *Solonenko et al.*, 1993]. "Doser" origin refers to *Doser* [1991a,b] modelings. Asterisks indicate fault plane solutions determined by several procedures (waveform modeling and first-motion determinations).
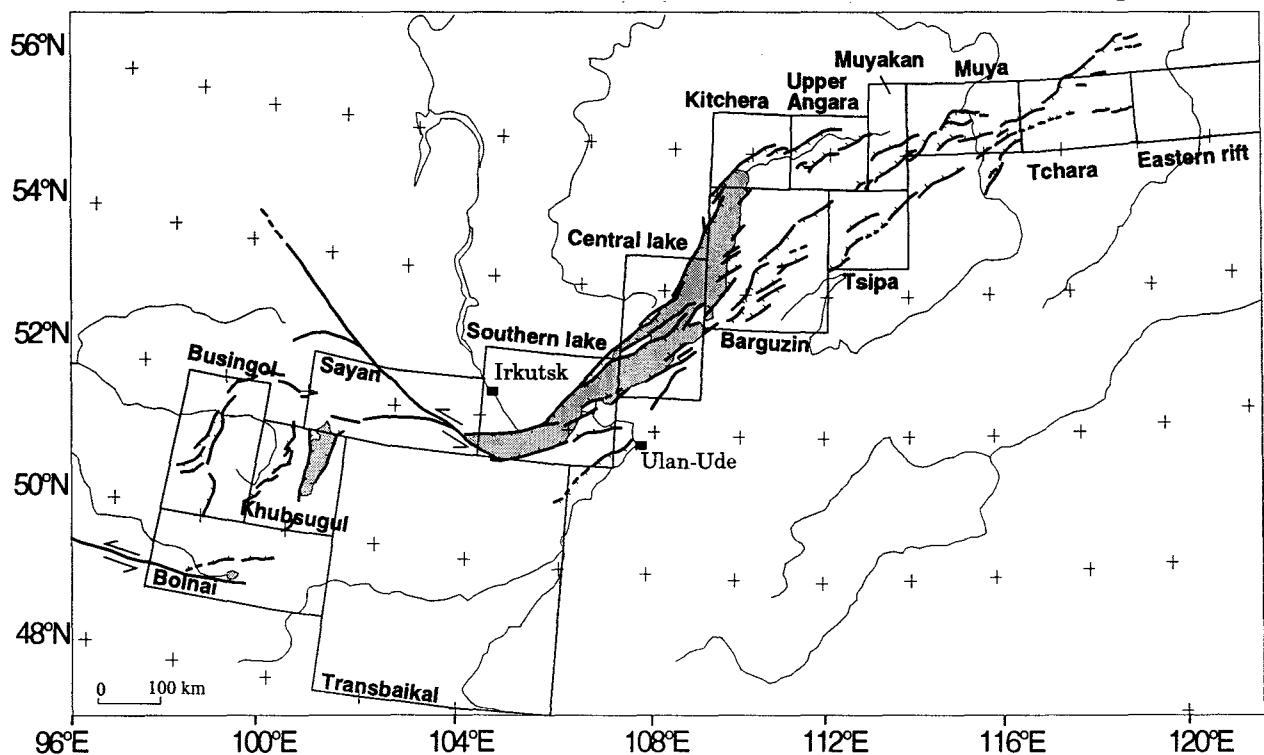
Figure 1. General map of the Baikal rift zone showing main active faults (bold lines) and 15 subareas (rectangles) corresponding to stress tensor determinations.
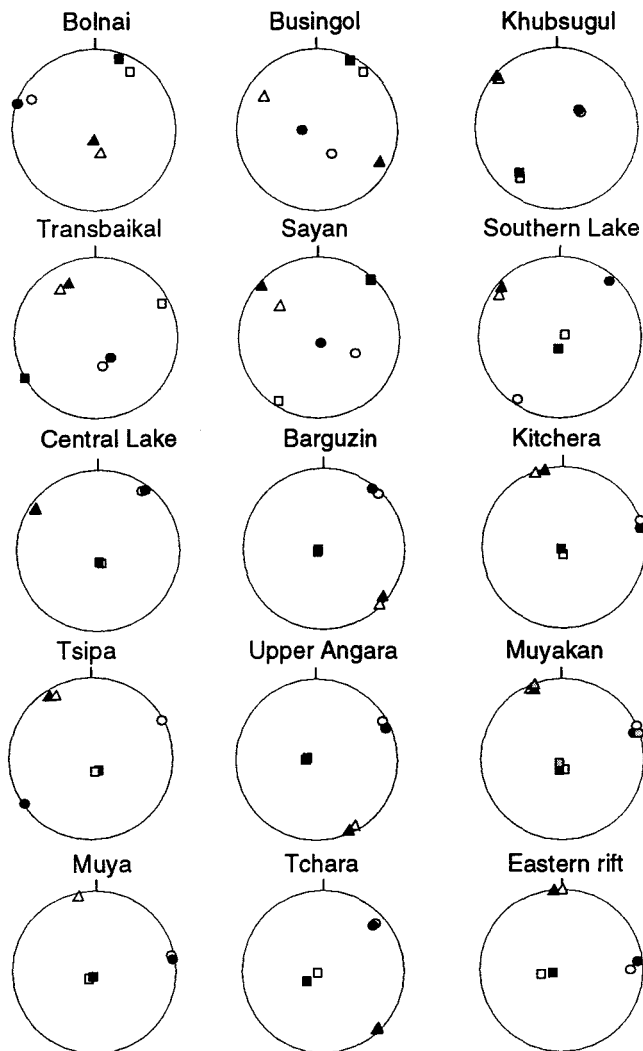
Figure 2. Main stress directions determined by numerical methods of *Carey and Mercier* [1987] (open symbols) and *Delvaux et al.* [1996] (solid symbols). Grey symbols for the Muyakan area are results after *Déverchère et al.* [1993]. Squares, circles and triangles are σ_1, σ_2, and σ_3 axes, respectively.

Predicted Slip Vectors

A stress tensor can be used to predict the direction and sense of movement on a given fault plane, especially in cases where field data are scarce or not reliable. *Ritz* [1994] developed a simple graphical method allowing one to deduce the slip vector on a given fault plane from the stress ellipsoid. We apply this method to several well-recognized faults in the BRZ, using the corresponding stress tensors previously obtained, in order to determine the predicted movement associated with the local stress field (Table 4). Compared to the use of focal mechanisms, this allows us to avoid possible large errors linked to uncertainties on positions of nodal poles: the stress tensor is well constrained by a large enough amount of data, and thus considerably reduces the uncertainty linked to the use of individual earthquakes. Moreover, active fault geometry is integrated during this procedure, which is supposed to provide more realistic estimates of slip vectors.

Active Fault Patterns

Detailed morphological and field analyses have been made in the NBR by *Houdry* [1994]. In this part of the rift, major fault scarps are numerous and shorter than in the SBR. They have been identified and measured either on the field or on satellite (SPOT) images. We gather the information on main fault direction and plunge in the NBR from this source (Table 4), considering the border faults of Kitchera, Upper Angara, Barguzin, Tsipa, Upper Muya, Muyakan, Muya, and Tchara basins as main active faults (Figure 5). In the NBR, faults exhibit high dips ranging between 50° and 60° [*Déverchère et al.*, 1993; *Houdry*, 1994]. Fault scarps strike from NS (locally in the Barguzin basin) to EW (in the Muya basin), but most of them strike approximately N60°E. This direction is inherited from anterift Paleozoic and Cenozoic history [*Sherman*, 1978; *Ermikov*, 1994; *Delvaux et al.*, 1996].

The Sayan-Tunka region is the southern limit of the studied area, because accuracies on fault geometry and stress tensors are not good enough to deduce slip vectors further southward. Deformation in the SBR is highly localized and mainly implies three major active faults: the South Baikal, Sayan, and Tunka faults. Information on their geometry comes from satellite (SPOT) images and Russian field studies [*Sherman*, 1992]. The South Baikal and Tunka faults strike about N80°E and dip southwards. The vertical dip of the Sayan fault is well evidenced by a nearly linear track, quite visible for 50 km from the southern tip of Baikal lake toward the NW.

In order to predict slip vectors on these structures, we make the assumption that the stress field determined from fault plane solutions is responsible for the movement along major faults. Indeed, seismicity distribution suggests that active deformation is preferably concentrated on these faults which correspond to inherited directions, except swarms that occur at the junction between the basins and may involve incipient neoforming structures [*Solonenko*, 1985; *Petit*, 1993]. Table 4 shows the resulting slip vectors predicted on these faults and the corresponding sense of movement. In order to estimate uncertainties on slip vector azimuths, we have computed the errors on predicted striations resulting from slight changes (equal to estimated uncertainties) applied to the stress tensor.

Slip Distribution

Figure 6 shows directions of horizontal movement predicted on main faults. Their azimuths vary from N73°E to N177°W, lineating different "kinematic provinces". Most of the predicted slip vectors (Table 4 and Figure 6) depict normal faulting, with a variable amount of strike-slip (e.g., sinistral for South Angara 2, Tchara, Barguzin 3, Primorsky 1 and Southern lake faults; dextral for Muyakan, Barguzin 1, and Taksimo faults). Sinistral strike-slip faulting with a small reverse component is found along the Sayan fault. In the SBR, including the southern half of the lake, slip directions are rather stable and range between N107°E and N121°E, except for the Tunka fault which exhibits a N73°E trending slip vector. This southern area of narrow and localized rifting is thus characterized by a relatively simple fault system exhibiting important sinistral movement. Note that this part of the rift is located close to the Paleozoic suture separating the Siberian craton from the Sayan-Baikal folded zone (Figure 5). The position of the rift at the emplacement of this major structural discontinuity [*Zamarayev and Ruzhich*, 1978; *Logatchev*, 1993]

$$R = \frac{\sigma 2 - \sigma 1}{\sigma 3 - \sigma 1}$$
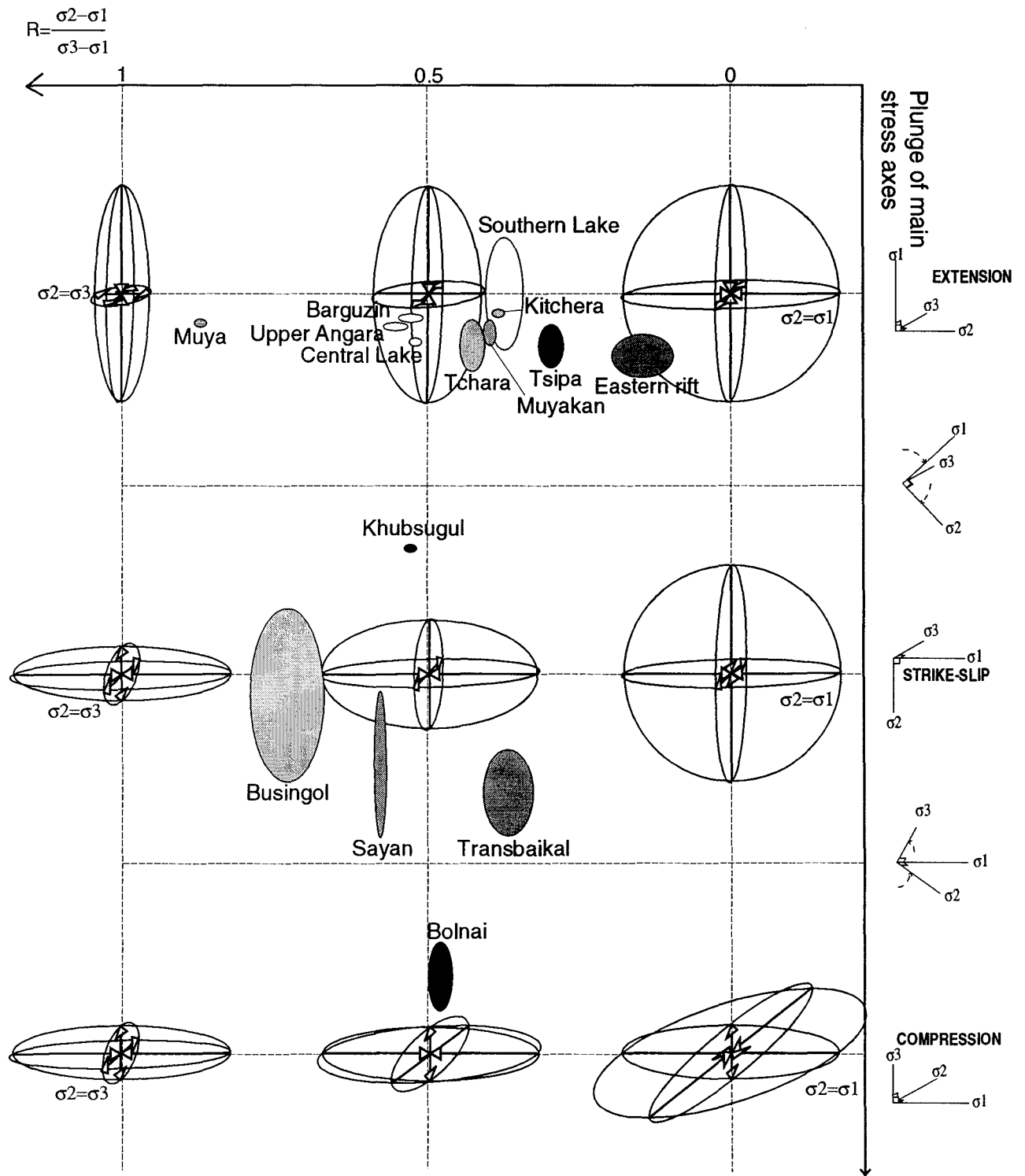
Figure 3. Diagram showing stress regime changes from radial extensive (upper-left ellipsoid) to radial compressive (lower-right ellipsoid) cases. R ratio varies horizontally. Inclination of main stress axes varies vertically. Ellipses correspond to uncertainty estimations on stress tensors. Grey levels refer to the quality factors: white, light grey, dark grey and black correspond to A, B, C, and D factors, respectively (see Table 2).

may explain the localized character of the deforming zone, as well as the homogeneous motion direction.

North of 54°N, slip distribution is much more variable (between N116°E and N177°W). Several features are standing

out in Figure 6: along the southern boundary of the deformed zone, predicted motions along the Barguzin and Tsipa faults are rather stable (around N145°E); meanwhile, the northern boundary exhibits more complex features which are characterized by
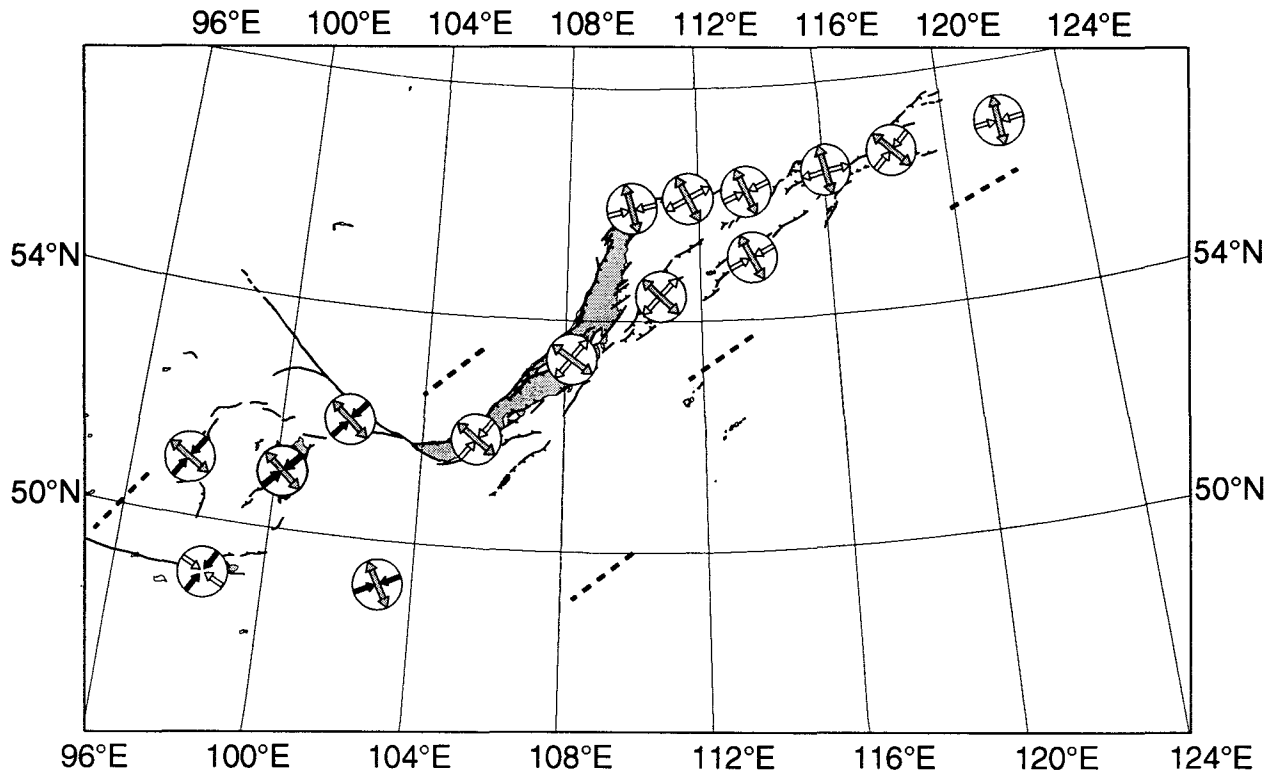
Figure 4. Map view of main horizontal stress directions in the Baikal rift (see Table 2). Grey arrows are σ_3; open divergent arrows are σ_2 when $R>0.5$; open convergent arrows are σ_2 when $R<0.5$; solid arrows are σ_1. Thick dashed line is regional S_{Hmax} direction after *Tapponnier and Molnar* [1979] and *Zoback* [1992].

progressive counterclockwise rotations of slip vectors from about N180°E to N130°E. From west to east, these rotations appear twice and indicate two main systems: the upper Angara (UA) area and the Muyakan-Upper Muya (M-UM) area (Figure 6). What is the meaning of such a complex movement pattern? Seismicity distribution in the NBR shows a pattern of seismic belts and swarms, clearly delimiting two aseismic zones. The first one includes the UA and M-UM areas, and the second one seems to correspond to the Barguzin-Tsipa (BT) region (Figure 7). Moreover, the boundary between UA and M-UM blocks is well underlined by a dextral shift of the corresponding seismic belts. From these observations, we infer that the deformation along the northern boundary of the NBR is characterized by block rotations, involving two crustal blocks rotating counterclockwise inside the deformed zone, relatively to the northern edge of the rift. The mean slip vector between the third block (BT) and the southern rift boundary has a constant azimuth.

Consistency With Previous Studies

These predicted motions along major rift faults are generally in good agreement with previous field observations and computed motions from cumulated Holocene displacements [see e.g., *Houdry*, 1994], and with previous local stress tensor determination [*Déverchère et al.*, 1993]. These studies (including this one) tend to indicate a dominant component of normal faulting in the NBR, which invalidates the strong sinistral component predicted by several authors [*Balla et al.*, 1991;

Ruppel et al., 1993] along the NBR faults. Oblique opening on the South Baikal fault and sinistral strike-slip motion on the Sayan fault are also consistent with previous results [see e.g., *Zonenshain and Savostin*, 1980; *Sherman*, 1978]. However, slip vector prediction shows two discrepancies with field analysis results. First, the computed fault motion on the Kitchera fault depicts a normal-dextral motion (Figure 6), while morphological field studies evidence normal-sinistral displacement [*Houdry*, 1994]. In order to explain this discrepancy, we assume that the Kitchera fault may not really belong to the UA block, and should be instead associated with the North Baikal basin system. The lack of seismicity in this latter area does not allow us to compute a stress tensor, but observed displacements along the North Baikal and Kitchera faults favor an average NW-SE trending slip. Second, the Tunka fault predicted slip vector depicts a reverse-sinistral motion; evidence for such movement is observed on the western part of the fault, but clear normal faulting is seen in its eastern half [see e.g., *McCalpin and Khromovskikh*, 1995]. The realistic sinistral strike-slip motion predicted for the Sayan fault leads us to believe that the stress tensor is reliable. The uncompatibility between predicted and observed motions on the eastern Tunka fault remains thus to be explained. It may result from a rapid change of the stress field in this region: the stress tensor computed on the western parts of Sayan and Tunka regions may be not suitable for slip vector computation in the eastern Tunka basin. A strain partitioning between the Sayan and Tunka faults may also be invoked.

Table 4. Predicted Slip Vectors on Main Active Faults of the BRZ

Name of the fault	Stress Tensor	Az. Pl.	Predicted Striation	Estimated 1σ
Tunka	Sayan	N80,60S	253-12	3
Sayan	Sayan	N120,90	301-27	9
Southern lake 1	Southern lake	N75,60S	107-42	11
Southern lake 2	Southern lake	N65,60N	285-48	5
Primorsky 1	Central lake	N50,60S	110-56	3
Primorsky 2	Central lake	N35,60S	135-60	5
Svyatoy Nos	Central lake	N30,60N	296-60	3
Barguzin 1	Barguzin	N25,60E	145-56	6
Barguzin 2	Barguzin	N40,60S	139-60	7
Barguzin 3	Barguzin	N65,60N	297-58	5
Kitchera	Kitchera	N60,60S	183-55	11
Dzelinda	Kitchera	N60,50S	172-48	10
Tsipa 1	Tsipa	N60,60N	330-60	15
Tsipa 2	Tsipa	N65,60N	325-60	15
North Angara 1	Upper Angara	N60,60S	163-59	4
North Angara 2	Upper Angara	N80,70S	134-66	3
South Angara 1	Upper Angara	N50,60N	340-58	7
South Angara 2	Upper Angara	N75,60N	314-56	6
Upper Muya 1	Muyakan	N60,60N	340-60	11
Upper Muya 2	Muyakan	N55,60N	343-59	12
Upper Muya 3	Muya	N50,60N	319-60	11
Muyakan 1	Muyakan	N50,60N	345-59	13
Muyakan 2	Muyakan	N75,60N	329-59	7
Muya 1	Muya	N90,60S	181-60	11
Muya 2	Muya	N40,60N	327-60	12
Taksimo	Muya	N40,60S	159-57	9
Tchara	Tchara	N65,60S	131-58	18

See Figure 5 for fault locations. Column 3 shows azimuth and plunge (in degrees) of the faults. Column 4 shows direction and plunge (in degrees) of predicted striations. Estimated 1σ (column 5) is the computed error on each slip vector determination (see Table 2), which underestimates the actual error, according to the quality factor assigned to each stress tensor determination (see Table 2). BRZ is Baikal Rift Zone.

Discussion: Comparison with the Asian Stress Field and Kinematics

The stress field study and inferred fault motions in the BRZ have allowed us to draw the main characteristics of rift dynamics and kinematics. How far does the regional (Asian) tectonic regime affect the rift characteristics, such as north-south contrast, and block rotations in the NBR? Previous studies have shown that global stress field patterns in central Asia are characterized by a continuous variation both in N-S and E-W directions [*Tapponnier and Molnar*, 1979; *Zoback*, 1992]: from west to east, S_{Hmax} orientation varies from NW-SE in the Pamir-Tarim region to N-S in the Gobi-Altai and NE-SW in the Tibet, Tsaidam, Nan-Shan, and Baikal zones; from south to north, the main outstanding feature is the progressive evolution of the stress field from compressional (Tarim, Tibet, Tien Shan) to wrench (Bolnai, Gobi-Altai) and finally extensional in the Baikal zone.

This study allows us to compare the local stress field variations in the Baikal rift zone to the broad-scale extensional stress regime previously described in this region. A first observation is that the average local S_{Hmax} directions are generally consistent with regional ones, suggesting that the same cause (the India-Asia collision) is responsible both for wrench-compressional tectonics existing in Mongolia and for the extensional regime governing the Baikal rift. However, some discrepancies are worth noting: in the SBR, while S_{Hmax} keeps striking NE-SW, the stress field abruptly changes from wrench-compressional to extensional; in the NBR, strong local S_{Hmax} deviations are found. We infer that inherited structures have an important influence on these local stress field changes: as reported before, the rapid change of tectonic regime happening in the SBR is geographically located at the place where the craton boundary direction changes (Figure 5); moreover, stress deviations in the whole rift are not randomly occurring but seem strongly linked to active fault tectonics at the same scale. In the extensional regime (Central lake, Upper Angara, Barguzin and Muya), systematic deviations of S_{Hmax} tend to trend parallel to normal fault directions. In the wrench-extensional regime (Southern lake, Kitchera, Tchara), the angle between S_{Hmax} and fault directions ranges between 13° and 38°. Finally, in the wrench-compressional regime (Bolnai, Sayan), S_{Hmax} becomes nearly perpendicular (65°-80°) to main fault orientations (Figure 8). Such stress reorientations close to major faults are also reported in the Mediterranean region by *Rebaï et al.* [1992]. Although broad-scale features of S_{Hmax} directions are relatively stable across the Asian continent, local influences are thus needed to explain the local stress field of the Baikal rift. This observation does not allow us to disregard the possible effect of deep lithospheric perturbations as the cause of second-order stress patterns. However, it highlights a strong relationship of stress field variations to the varying geometry of active faults and ancient sutures, suggesting that preexisting structures at least partly control the state of stress of the rift.

Such interaction between local stress patterns and local structures finds its expression in the deformation of the rift zone, allowing us to draw a similar comparison with the global strain of Asia. The latter is still a subject of controversy; especially, the role of strike-slip faulting in the accommodation of India-Asia convergence is highly debated. According to several authors, extrusion processes involving localized deformation along major strike-slip faults are dominant [see e.g., *Tapponnier et al.*, 1982; *Peltzer and Tapponnier*, 1988; *Avouac and Tapponnier*, 1993]. On the other hand, some authors have modelled a more continuous style of deformation, where strike-slip faulting plays a limited role in the accommodation of plate motion [see e.g., *Houseman and England*, 1993]. Recently, from modelling of earthquake moment tensors, *Holt et al.* [1995] have proposed that strike-slip faulting only accommodates the rotation of the South China block relative to Siberia. Generally, although several authors agree that the India-Asia collision effects extend as far as in the Baikal region [see e.g., *Molnar and Tapponnier*, 1975; *Molnar and Deng*, 1984], only few models predict consequent horizontal strains in the BRZ. *Molnar and Deng* [1984] use large earthquakes to predict an average convergence azimuth of N36°E between Mongolia and Siberia. *Holt et al.* [1995] also modelled an average SW-NE motion of Mongolia relative to Siberia, south of the Baikal Rift Zone. In spite of large uncertainties, both models favor SW-NE convergence between Mongolia (Amurian plate) and Siberia, which is quite consistent with the maximum horizontal stress direction observed.

At a more detailed scale, the BRZ depicts abrupt lateral strain variations. From south to north, reverse, oblique, and normal motions follow each other. It thus remains to explain how far the rift deformation described here fits or does not fit the kinematic model of central Asia, that is, what are the causes of opening of the rift in a context of SW-NE plate convergence? From a purely
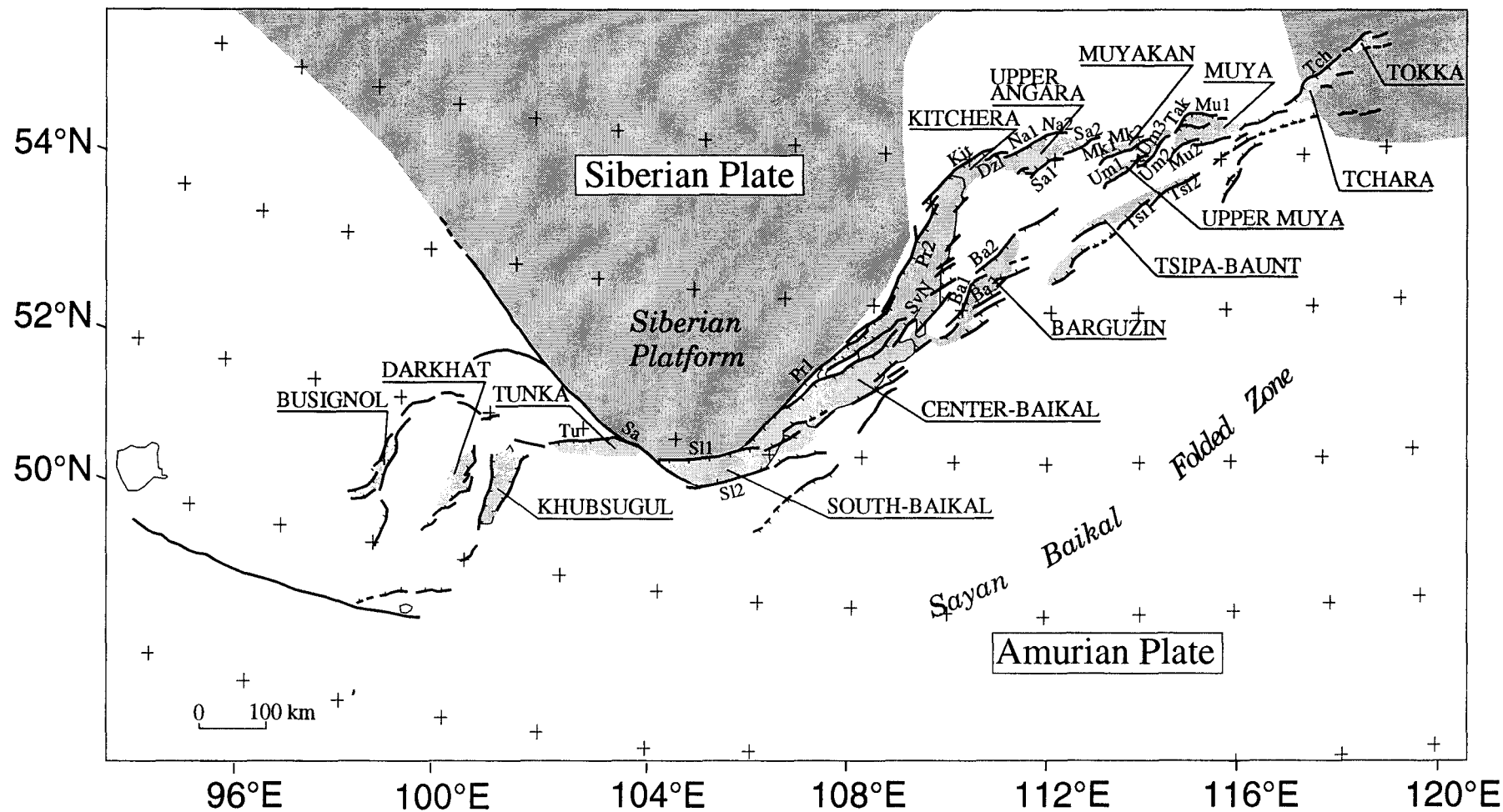
Figure 5. Simplified structural sketch of the Baikal rift area. Grey areas correspond to Siberian craton. Names of the basins are underlined. Small abreviations refer to faults used for striation prediction: Sa, Sayan; Sl1, Southern lake 1; Sl2, Southern lake 2; Pr1, Primorsky 1; Pr2, Primorsky 2; SvN, Svyatoy Nos; Ba1, Barguzin 1; Ba2, Barguzin 2; Ba3, Barguzin 3; Dzl, Dzelinda; Kit, Kitchera; Tsi1, Tsipa 1; Tsi2, Tsipa 2; Na1, North Angara 1; Na2, North Angara 2; Sa1, South Angara 1; Sa2, South Angara 2; Mk1, Muyakan 1; Mk2, Muyakan 2 ; Um1, Upper Muya 1; Um2, Upper Muya 2; Um3, Upper Muya 3; Mu1, Muya 1; Mu2, Muya 2; Tak, Taksimo; Tch, Tchara; Tu, Tunka [after *Logatchev*, 1993; *Houdry*, 1994].
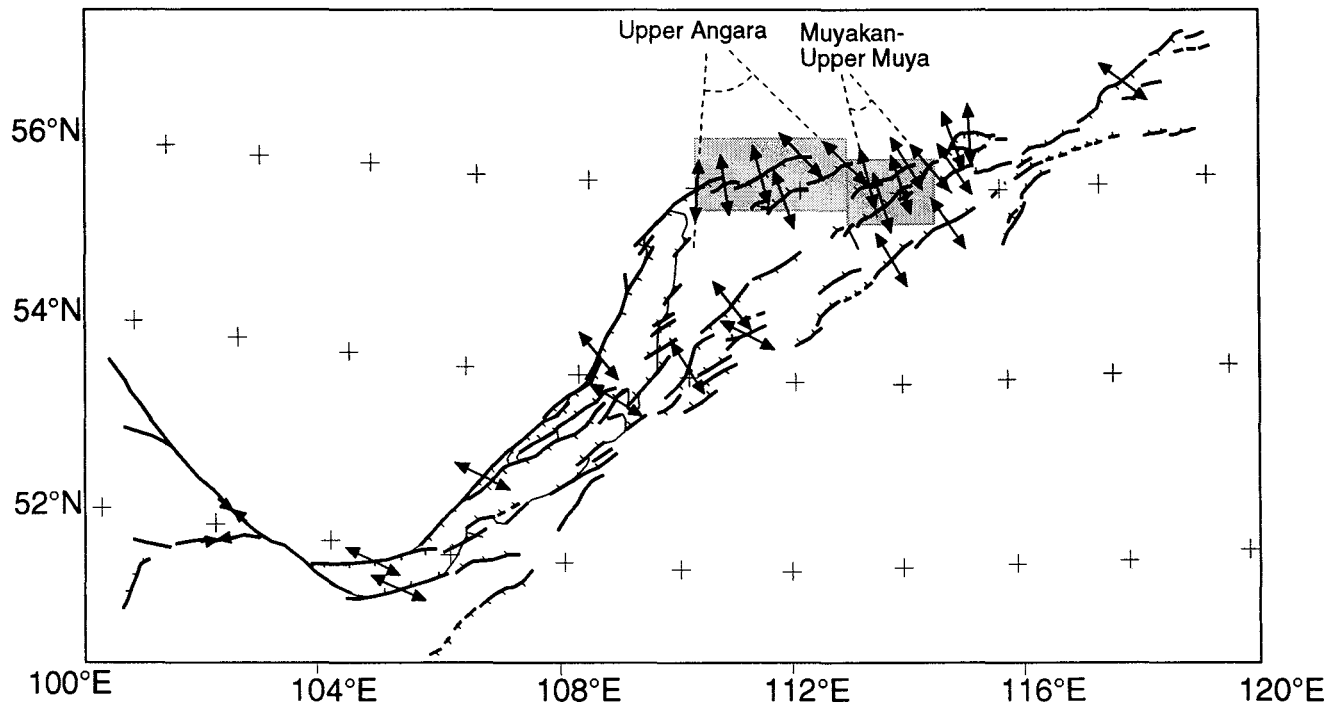
Figure 6. Map view of the 27 predicted slip vector azimuths (see Table 4 and text). Divergent and convergent arrows correspond to normal and reverse motions, respectively. Grey rectangles are the areas of counterclockwise slip vector rotations described in the text.

geometrical point of view, a rather satisfying explanation may be found when considering the particular shape of the hardly deformable Siberian shield bounding the SBR (Figure 5). In the westernmost part of the rift, if we assume an average N40°E convergence vector between the Amurian and Siberian plates, then the NW-SE edge of the rigid platform may strongly resist the northeastward propagation of the compressional strain field. Consequently, reverse and sinistral faulting along the Sayan fault accommodates part of the convergence (Figure 9a). Actually, strike-slip faulting is predominant on the Sayan fault: it may be a result of a relative eastwards "escaping" of the Amurian plate. This kind of deformation is also predominant inside western Mongolia, especially along the major sinistral faults of Bolnai and Bogd [*Baljinnyam et al.*, 1993]. The corner shape of the craton, at the southern tip of the Baikal lake, must play an important role in the accommodation of relative convergence motions: the Southern lake region (which is the deepest rift depression) is located against the SW-NE craton edge which is roughly parallel to the convergence direction. The opening of this part of the rift thus looks like a large-scale tension crack opening, where one border of the crack is resistant and the other one moves eastward (Figure 9b). Finally, the NBR is developing inside an indentation of the Siberian shield: most of the basins of the NBR are located in the Sayan-Baikal mobile belt, but both the large SW end and the sharp NE end of the NBR are bounded by the Siberian craton. We thus propose that, in the NBR too, the shield geometry may have an indirect influence on the rift evolution, tending to resist the northeastward propagation of deformation (Figure 9c). This influence has already been noticed by *Sherman* [1978, 1992] and *Logatchev* [1993], who however point out that rift structures are more likely to propagate

northward than southward. The rift zone seems more able to increase in width (i.e., inside the weakened folded zone) than in length (i.e., inside the resistant shield): this wide deformed zone could indicate large-scale extensional "cracking" of the lithosphere, as already suggested by *Burov et al.* [1994], inside which the opening gives rise to block rotations.

If these hypotheses are a possible way to explain observed motions in the Baikal rift, the overall three-dimensional behavior of the rift involves much more complex phenomena. For instance, the clear partitioning of the rift into two different zones especially suggests that anterift history may also strongly control the rheological behavior of the BRZ. Indeed, the rift is located on two main zones of weakened crust: the Paleozoic suture and the folded zone. The nature, as well as the dimension of these two weaknesses are quite different: one is a structural narrow boundary, the other one is a wide area of thickened crust, which thus offers a lower strength to extensional forces [*Kusznir and Park*, 1987]. When its orientation is favorable (i.e., in the SBR), the rift closely follows the suture between the Siberian craton and the Sayan-Baikal folded belt; when it becomes unfavorable (like in the NBR), it propagates inside the folded zone. The rheological contrast of these two deforming zones may thus also partly explain the location and varying geometry of the BRZ [*Houdry*, 1994]. Moreover, in the present study, we take the India-Asia collision as the only source of stress in the BRZ; we believe that it is an acceptable simplification for qualitative models like this one. However, two other factors must be taken into account to infer a quantitative model of deformation in this zone: first, the thermal effect resulting from possible lithospheric thinning beneath the Baikal region may create a weakening of the lithosphere [*Lysak*, 1992; *Nicolas et al.*, 1994]; second, the whole
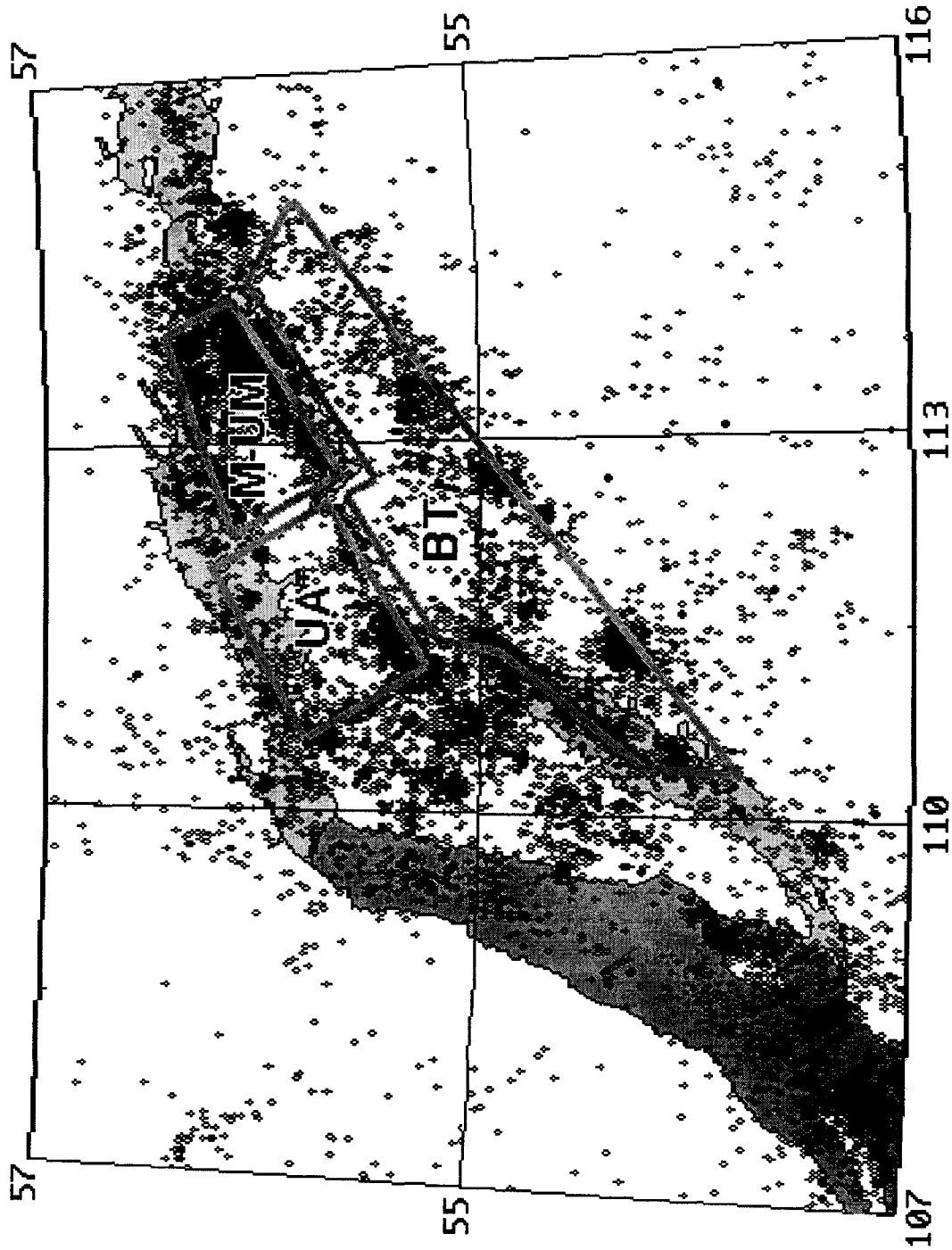
Figure 7. Seismicity map of the North Baikal Rift (NBR). All magnitude earthquakes located by the permanent russian network from 1960 to 1992 (about 5000 events) are shown. Lake Baikal and rift basins are shaded. Aseismic blocks delimited by seismic belts are drawn in order to compare with slip vector rotations shown on Figure 6.
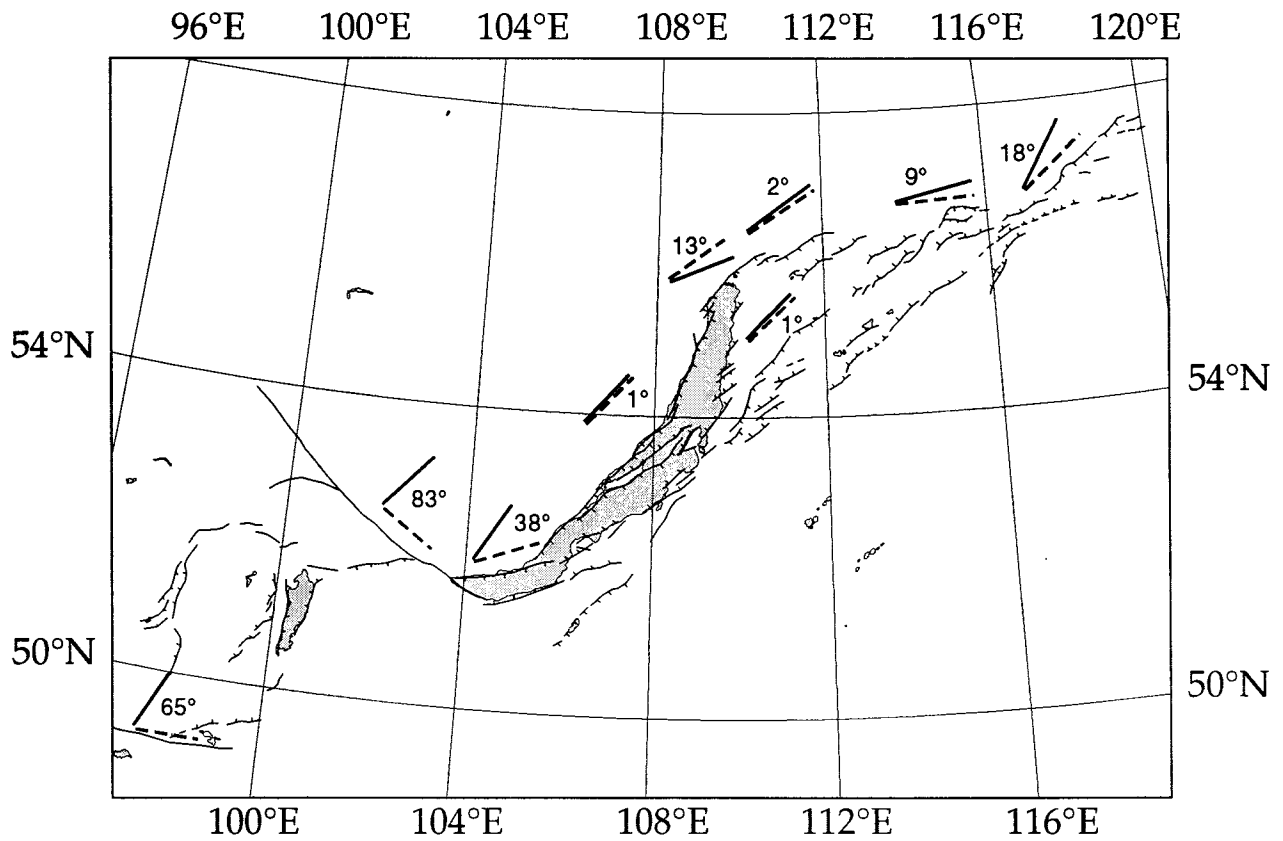
Figure 8. Map of angular differences between S_{Hmax} directions (thick lines) and active fault strikes (dashed lines), referred to the active fault pattern of the rift area (thin lines).
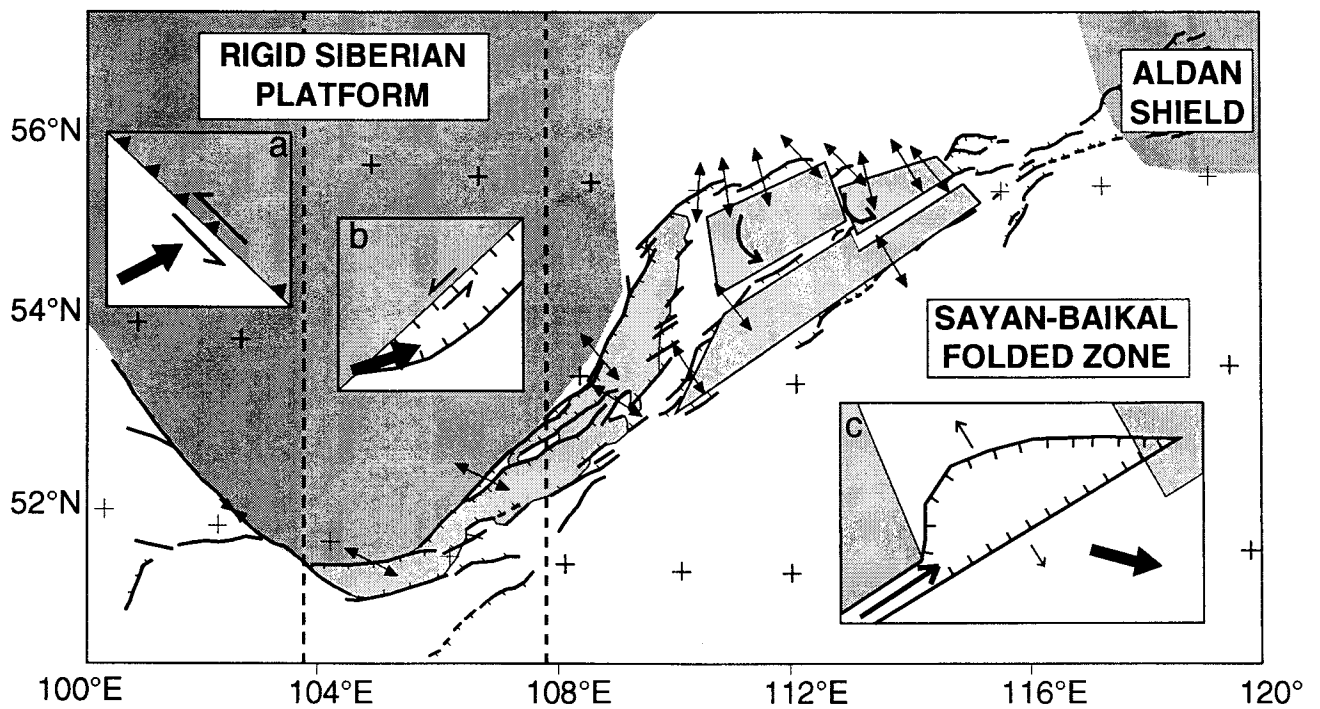
Figure 9. Schematic interpretation of the predicted motions in terms of rift deformation. Thick solid arrows in box a, box b, and box c are mean relative motions between Amurian and Siberian plates, extrapolated after *Holt et al.* [1995] and *Houdry* [1994]. Shaded areas are blocks depicted on Figure 7. Double arrows are slip vectors selected from Figure 6. See text for details.

eastern border of the continent is bounded by subduction trenches whose tensional effect is not neglectable and can propagate far into the plate interior, contributing to its weakening [*Whittaker et al.*, 1992]. Under these conditions, the forces resulting from the India-Asia collision, although strongly attenuated when reaching the remote Baikal region, can be important enough to produce a rift opening at this place. Consequently, the debate between passive and active rifting has a limited meaning here, as already mentioned elsewhere by *Nicolas et al.* [1994].

References

Angelier, J., Determination of the mean principal stresses for a given fault population, *Tectonophysics, 56,* 17-26, 1979.

Angelier, J., and P. Mechler, Sur une méthode graphique de recherche des contraintes principales également utilisable en tectonique et en sismologie: La méthode des dièdres droits, *Bull. Soc. Géol. Fr., XIX,* 651-652, 1977.

Avouac, J.-P., and P. Tapponnier, Kinematic model of deformation in central Asia, *Geophys. Res. Lett., 20,* 895-898, 1993.

Baljinnyam, I., A. Bayasgalan, B. A. Borisov, A. Cisternas, M. G. Dem'yanovich, L. Ganbaatar, V. M. Kochetkov, R. A. Kurushin, P. Molnar, H. Philip, and Y. Y. Vashchilov, Ruptures of major earthquakes and active deformation in Mongolia and its surroundings, 62 pp., *Geol. Soc. Am. Mem. 181,* 1993.

Balla, Z., M. Kuzmin, and K. Levi, Kinematics of the Baikal opening: Results of modelling, *Ann. Tectonic., 1,* 18-31, 1991.

Bosworth, W., M. R. Strecker, and P. M. Blisniuk, Integration of east African paleostress and present-day stress data: Implication for continental stress field dynamics, *J. Geophys. Res., 97,* 11,851-11,865, 1992.

Burov, E. B., F. Houdry, M. Diament, and J. Déverchère, A broken plate beneath the Baikal rift zone revealed by gravity modelling, *Geophys. Res. Lett., 21,* 129-132, 1994.

Carey-Gailhardis, E., and J.-L. Mercier, A numerical method for determining the state of stress using focal mechanisms of earthquake populations: Application to Tibetan teleseisms and microseismicity of southern Peru, *Earth Planet. Sci. Lett., 82,* 165-179, 1987.

Cornet, F. H., and D. Burlet, Stress field determination in France by hydraulic tests in boreholes, *J. Geophys. Res., 97,* 11,829-11,850, 1992.

Davy, P., and P. R. Cobbold, Indentation tectonics in nature and experiment, 1, Experiments scaled for gravity, *Bull. Geol. Inst. Univ. Uppsala, N.S. 14,* 129-141, 1988.

Delvaux, D., A. Melnikov, and V. Ermikov, Paleostress reconstruction and geodynamics of the Baikal region, Central Asia, I, Paleozoic and Mesozoic pre-rift evolution, *Tectonophysics, 252,* 61-101, 1996.

Déverchère, J., F. Houdry, M. Diament, N. V. Solonenko, and A. V. Solonenko, Evidence for a seismogenic upper mantle and lower crust in the Baikal rift, *Geophys. Res. Lett., 18,* 1099-1102, 1991.

Déverchère, J., F. Houdry, N. V. Solonenko, A. V. Solonenko, and V. A. Sankov, Seismicity, active faults and stress field of the North Muya region, Baikal rift: New insights on the rheology of extended continental lithosphere, *J. Geophys. Res., 98,* 19,895-19,912, 1993.

Diament, M., and M. G. Kogan, Long wavelength gravity anomalies and the deep thermal structure of the Baikal rift, *Geophys. Res. Lett., 17,* 1977-1980, 1990.

Doser, D. I., Faulting within the western Baikal rift as characterized by earthquake studies, *Tectonophysics, 196,* 87-107, 1991a.

Doser, D. I., Faulting within the eastern Baikal rift as characterized by earthquake studies, *Tectonophysics, 196,* 109-139, 1991b.

Dziewonski, A. M., and J. H. Woodhouse, An experiment in the systematic study of global seismicity: Centroid-moment tensor solutions for 201 moderate and large earthquakes of 1981, *J. Geophys. Res., 88,* 3247-3271, 1983.

Ermikov, V. D., Mesozoic precursors of the Cenozoic rift structures of Central Asia, *Bull. Centres Rech. Explor.-Prod. Elf Aquitaine, 18,* 123-134, 1994.

Gao, S., P. M. Davis, H. Liu, P. D. Slack, Y. A. Zorin, N. A. Logatchev, M. G. Kogan, P. D. Burkholder, and R. P. Meyer, Asymmetric upwarp of the asthenosphere beneath the Baikal rift zone, Siberia, *J. Geophys. Res., 99,* 15,319-15,330, 1994.

Gephart, J. W., and D. W. Forsyth, An improved method for determining the regional stress tensor using earthquake focal mechanism data: Application to the San Fernando earthquake sequence, *J. Geophys. Res., 89,* 9305-9320, 1984.

Golenetsky, S. I., Problems of the seismicity of the Baikal rift zone, *J. Geodyn., 11,* 293-307, 1990.

Hartse, H. E., M. C. Fehler, R. C. Aster, J. S. Scott, and F. L. Vernon, Small-scale stress heterogeneity in the Anza seismic gap, southern California, *J. Geophys. Res., 99,* 6801-6818, 1994.

Hippolyte, J.-C., J. Angelier, and F. Roure, A major geodynamic change revealed by Quaternary stress patterns in the Southern Apennines (Italy), *Tectonophysics, 230,* 199-210, 1994.

Holt, W. E., M. Li, and A. J. Haines, Earthquake strain rates and instantaneous relative motions within central and eastern Asia, *Geophys. J. Int., 122,* 569-593, 1995.

Horiuchi, S., G. Rocco, and A. Hasegawa, Discrimination of fault planes from auxiliary planes based on simultaneous determination of stress tensor and large number of fault plane solutions, *J. Geophys. Res., 100,* 8327-8338, 1995.

Houdry, F., Mécanismes de l'extension continentale dans le rift Nord Baikal, Sibérie, 356 pp., Thèse de Doctorat, Univ. Pierre et Marie Curie (Paris VI), 1994.

Houseman, G., and P. England, Crustal thickening versus lateral expulsion in the India-Asian continental collision, *J. Geophys. Res., 98,* 12,233-12,249, 1993.

Kusznir, N. J. and R. G. Park, 1987, The extensional strength of the continental lithosphere: Its dependence on geothermal gradient, and crustal composition and thickness, in *Continental Extensional Tectonics, Geol. Soc. Spec. Publ.,* M. P. Coward, J. F. Dewey and P. L. Hancock eds, 35-52.

Logatchev, N. A., History and geodynamics of the Lake Baikal Rift in the context of the Eastern Siberia rift system: A review, *Bull. Centres Rech. Explor.-Prod. Elf Aquitaine, 17,* 353-370, 1993.

Lysak, S. V., Heat flow variations in continental rifts, *Tectonophysics, 208,* 309-323, 1992.

McCalpin, J. P., and V. S. Khromovskikh, Holocene paleoseismicity of the Tunka fault, Baikal rift, Russia, *Tectonics, 14,* 594-605, 1995.

McKenzie, D. M., The relation between fault plane solutions for earthquakes and the direction of the principal stresses, *Bull. Seismol. Soc. Am., 59,* 591-601, 1969.

Michael, A. J., Use of focal mechanisms to determine stress: A control study, *J. Geophys. Res., 92*, 357-368, 1987.

Molnar, P., and Q. Deng, Faulting associated with large earthquakes and the average rate of deformation in central and eastern Asia, *J. Geophys. Res., 89*, 6203-6227, 1984.

Molnar, P., and P. Tapponnier, Cenozoic tectonics of Asia: Effects of a continental collision, *Science, 189*, 419-426, 1975.

Nicolas, A., U. Achauer, and M. Daignières, Rift initiation by lithospheric rupture, *Earth Planet. Sci. Lett., 123*, 281-298, 1994.

Peltzer, G., and P. Tapponnier, Formation and evolution of strike-slip faults, rifts and basins during the India-Asia collision: An experimental approach, *J. Geophys. Res., 93*, 15,095-15,117, 1988.

Petit, C., Analyse de séquences sismiques par relocalisation: Application au rift Nord-Baïkal et interprétation tectonique, 57 pp., *Rapp. de DEA de l'Univ. Pierre et Marie Curie (Paris VI)*, 1993.

Petit, C., and J. Déverchère, Velocity structure of the northern Baikal rift, Siberia, from local and regional earthquake travel times, *Geophys. Res. Lett., 22*, 1677-1680, 1995.

Petit, C., J. Déverchère, E. Calais, A. Deschamps, K. G. Levi, V. A. Sankov, V. V. Ruzhich, A. I. Miroshnichenko, N. V. Solonenko, and O. Petukhov, Active tectonics, stress tensor analysis, and first GPS survey of the southern Baikal rift, *EOS Trans. AGU*, Fall Meet. suppl., *75 (44), 181*, 1994.

Rebaï, S., H. Philip, and A. Taboada, Modern tectonic stress field in the Mediterranean region: Evidence for variation in stress directions at different scales, *Geophys. J. Int., 110*, 106-140, 1992.

Richardson, R. M., Ridge forces, absolute plate motions, and the intraplate stress field, *J. Geophys. Res., 97*, 11,739-11,748, 1992.

Ritz, J.-F., Determining the slip vector by graphical construction: Use of a simplified representation of the stress tensor, *J. Struct. Geol., 16*, 737-741, 1994.

Rivera, L., and A. Cisternas, Stress tensor and fault plane solutions for a population of earthquakes, *Bull. Seismol. Soc. Am., 80*, 600-614, 1990.

Ruppel, C. D., M. G. Kogan, and M. K. McNutt, Implications of new gravity data for Baikal rift zone structure, *Geophys. Res. Lett., 20*, 1635-1638, 1993.

Shamir, G., M. D. Zoback, and C. B. Barton, In situ stress orientation near the San Andreas fault: Preliminary results to 2.1 km depth from the Cajon Pass scientific drillhole, *Geophys. Res. Lett., 15*, 989-992, 1988.

Sherman, S. I., Faults of the Baikal rift zone, *Tectonophysics, 45*, 31-39, 1978.

Sherman, S. I., Faults and tectonic stresses of the Baikal rift zone, *Tectonophysics, 208*, 297-307, 1992.

Solonenko, A. V., N. V. Solonenko, V. I. Melnikova, B. M. Kuzmin, O. A. Kuchai, and S. S. Sukhanova, Stresses and fault plane motions of earthquakes in Siberia and Mongolia (in Russian), *Seismicity and seismic zoning of Northern Eurasia*, IFE RAS, *1, 113-122*, 1993.

Solonenko, N. V., The energy released in seismic sequences of the Baikal rift zone, *Proc. 3rd International Symposium on the analysis of seismicity and seismic risk, Liblice Castle, Prag, Czechoslovakia*, 216-224, 1985.

Solonenko, V. P., *Seismic regional division of eastern Siberia and its geological-geophysical base (in Russian)*, Nauka, Novosibirsk, 92-162, 1977.

Tapponnier, P., and P. Molnar, Active faulting and Cenozoic tectonics of the Tien Shan, Mongolia and Baykal regions, *J. Geophys. Res., 84*, 3425-3459, 1979.

Tapponnier, P., G. Peltzer, A. Y. Le Dain, R. Armijo, and P. R. Cobbold, Propagating extrusion tectonics in Asia: New insights from simple experiments with plasticine, *Geology, 10*, 611-616, 1982.

Whittaker, A., M. H. P. Bott, and G. D. Waghorn, Stresses at plate boundary forces associated with subduction plate margins, *J. Geophys. Res., 97*, 11,933-11,944, 1992.

Xu, Z., W. Suyun, H. Yurui, and G. Ajia, Tectonic stress field of China inferred from a large number of small earthquakes, *J. Geophys. Res., 97*, 11,867-11,878, 1992.

Zamarayev, S. M., and V. V. Ruzhich, On relationships between the Baikal and ancient structures, *Tectonophysics, 45*, 41-47, 1978.

Zoback, M. L., First- and second-order patterns of stress in the lithosphere: The World Stress Map Project, *J. Geophys. Res., 97*, 11,703-11,728, 1992.

Zoback, M. D., and G. C. Beroza, Heterogeneous slip and stress release in the Loma Prieta earthquake, II, Evidence for near frictionless faulting and complete co-seismic stress drop, *EOS Trans. AGU, Fall Meeting suppl., 72 (44)*, 309, 1991.

Zoback, M. L., et al., Global patterns of tectonic stresses, *Nature, 341*, 291-298, 1989.

Zonenshain, L. P., and L. A. Savostin, Geodynamics of the Baikal rift zone and plate tectonics of Asia, *Tectonophysics, 76*, 1-45, 1980.

J. Déverchère, F. Houdry, and C. Petit, Laboratoire de Géodynamique Sous-Marine, Observatoire Océanologique, La Darse, BP48, 06230 Villefranche-sur-Mer, France. (e-mail: jack@ccrv.obs-vlfr.fr)

V. I. Melnikova, V. A. Sankov, Institute of the Earth's Crust, Lermontov St. 128, Irkutsk 664033, Russia. (e-mail: san@cora.irkutsk.su)

D. Delvaux, Royal Museum for Central Africa, Leuvensesteenweg, 13, B-3080 Tervuren, Belgium. (e-mail: ddelvaux@vub.ac.be)